P-terminated InP(001) surfaces: Surface band bending and reactivity to water

D. C. Moritz,[1,*] I. A. Ruiz Alvarado,[2,*] M. A. Zare Pour,[3] A. Paszuk,[3] T. Frieß,[1] E. Runge,[3] J. P. Hofmann,[1] T. Hannappel,[3] W. G. Schmidt,[2,†] and W. Jaegermann[1,3,‡]

[1] *Technical University of Darmstadt, Department of Materials and Earth Sciences, Surface Science Laboratory, Otto-Berndt-Straße 3, 64287 Darmstadt, Germany*

[2] *Universität Paderborn, Lehrstuhl für Theoretische Materialphysik, Warburger Straße 100, 33095 Paderborn, Germany*

[3] *Technische Universität Ilmenau, Institut für Physik, Gustav-Kirchhoff-Straße 5, 98693 Ilmenau, Germany*

(Dated: July 18, 2022)

Stable InP(001) surfaces are characterized by fully occupied and empty surface states close to the bulk valence and conduction band edges, respectively. The present photoemission data show, however, a surface Fermi level pinning only slightly below the mid-gap energy that gives rise to an appreciable surface band bending. By means of density-functional theory calculations, it is shown that this apparent discrepancy is due to surface defects that form at finite temperature. In particular, the desorption of hydrogen from metalorganic vapor phase epitaxy grown P-rich InP(001) surfaces exposes partially filled P dangling bonds that give rise to band gap states. These defects are investigated with respect to surface reactivity in contact with molecular water by low-temperature water adsorption experiments using photoemission spectroscopy and are compared to our computational results. Interestingly, these hydrogen related gap-states are robust with respect to water adsorption, provided that water does not dissociate, due to missing adsorption sites in close neighborhood.

I. INTRODUCTION

Due to their promising photovoltaic performances, III-V photoabsorbers such as InP gain a lot of attraction with respect to their application in the field of photoelectrochemical water splitting [1, 2]. However, the role of surface defects, especially in contact with the liquid electrolyte, is still not fully understood, impeding further efficiency improvement of the photoelectrode. For that reason, the focus was redirected to the electrochemical interface of the semiconducting photoabsorber and the liquid electrolyte in the last decade [3–5]. Furthermore, the interaction of InP as photoabsorber with water is also of high relevance when depositing conductive oxides as electrochemical buffer layer using atom layer deposition (ALD) where water frequently is used as oxide precursor [6, 7].

We, therefore, investigated the P-rich InP(001) surface and its interaction with water using X-ray (XPS) and ultraviolet (UPS) photoemission spectroscopy as well as low energy electron diffraction (LEED). In particular, we focus on the surface Fermi level position, which is found to be pinned close to mid-gap. *Ab initio* thermodynamics and band structure calculations show that this is related to surface defects. Furthermore, the surface reactivity of the defective surface in contact with water is investigated by modeling the semiconductor-electrolyte contact under ultra-high vacuum (UHV) using the *"frozen electrolyte"* approach [8].

* These authors contributed equally to this work.
† Corresponding authors; W.G.Schmidt@upb.de
‡ Corresponding authors; Jaegermann@surface.tu-darmstadt.de

II. EXPERIMENTAL DETAILS

Homoepitaxial InP (001) was grown on p-type InP (001) (Zn doped, $2-2.3\cdot10^{18}$ cm^{-3} with 2 ° miscut toward $< 111 >$ direction) in a horizontal-flow metalorganic vapor phase epitaxy (MOVPE) reactor (Aixtron, AIX-200) modified to enable a contamination-free transfer to UHV using H_2 as carrier gas. Tert-butylphospine (TBP) and trimethylindium (TMIn) were used as precursors. Diethylzinc (DEZn) was used as a p-dopant source for grown InP(001) epilayer. Molar flow of DEZn was adjusted to ensure a carrier concentration of $2\cdot10^{18}$ cm^{-3} in the InP(001) epilayer, which was finally confirmed by electrochemical capacitance voltage profiling. The growth was monitored by reflection anisotropy spectroscopy (RAS) which allows the specific preparation of the P-rich surface (see [9, 10] for details). After sample preparation at TU Ilmenau, the sample was transferred via an UHV transfer shuttle with a base pressure $\leq 5\cdot10^{-10}$ [11] to TU Darmstadt.

X-ray photoemission spectroscopy (XPS) measurements were conducted normal to the surface with a SPECS PHOIBOS 150 spectrometer in *medium area* mode using a monochromatic Al Kα X-ray source (Focus 500 with XR50M (*SPECS*) with $h\nu$ = 1486.74 eV) as part of the *DAISY-FUN* cluster tool. Survey and detail spectra were measured in fixed analyzer transmission mode with a pass energy of 20 eV (step size of 0.5 eV) and 10 eV (step size of 0.05 eV), respectively. The spectrometer was calibrated by yielding the Fermi level edge of Au, Ag, Cu to 0 eV binding energy as well as $Au4f_{7/2}$ at 83.98 eV, $Ag3d_{5/2}$ at 368.26 eV and $Cu2p_{3/2}$ at 932.67 eV binding energy with deviations $\leq$ 50 meV. Ultraviolet photoemission spectroscopy (UPS) measure-

ments were conducted on the same spectrometer with pass energy of 5 eV (step size of 0.05 eV) using the HIS 13 Mono (*Focus GmbH*) as monochromatic HeII-source with $h\nu = 40.81$ eV normal to the surface. Low-temperature water adsorption has been performed by cooling the manipulator with liquid nitrogen leading to a substrate temperature of -176 °C. Subsequently, the cooled manipulator was separated to another chamber with a base pressure of $< 10^{-9}$ mbar and the sample was exposed to water using a leak valve. The dosage was controlled by the water pressure and the exposure time where a dose of 100 s at 10^{-8} mbar is defined as 1 L (Langmuir).

III. COMPUTATIONAL DETAILS

Density-functional theory (DFT) calculations are performed using the Vienna Ab-Initio Simulation Package (VASP) [12]. The electron exchange and correlation effects are treated within the generalized gradient approximation (GGA) using the PBE functional [13]. The electron-ion interaction is described by the projector-augmented wave (PAW) scheme [14, 15]. The surfaces are modeled using periodic supercells that contain 12 atomic layers. A vacuum region of about 15 Å is used to decouple the material slab from its periodic image. The electric field in the vacuum region resulting from the two nonequivalent slab surfaces is quenched using a dipole correction. The wave functions are expanded into plane waves up to an energy cutoff of 500 eV. The surface Brillouin zone is sampled using a Γ centered 4×4 k-point mesh. All interfaces are structurally relaxed until the forces acting on the atoms are below 0.02 eV/Å. Band structure calculations for defect-containing 2×2 surface unit cells were performed within 4×4 translational symmetry, in order to reduce spurious defect-defect interactions.

In order to determine the most favorable adsorption sites for water molecules and hydroxyl groups, potential energy surfaces (PES) are calculated using a mesh of 64 equidistant points. Here, the oxygen lateral degrees of freedom are constrained, while all other degrees of freedom are allowed to relax fully. Two and three different starting configurations are probed for hydroxyl group and water molecule, respectively, at each mesh point.

The defect density N_i of some specific defect i is obtained from the Boltzmann distribution according to

$$\frac{N_i}{N} = \frac{e^{-\Delta G_f^i / k_B T}}{1 + \sum_k e^{-\Delta G_f^k / k_B T}} \tag{1}$$

where N is the total number of defect sites and T the temperature. The Gibbs free defect formation energy is given by

$$\Delta G_f(p,T) = G_{\mathrm{def}}(p,T) - G_{\mathrm{ideal}}(p,T) - \sum_j \Delta n_j \mu_j(p,T). \tag{2}$$

Here G_{def} and G_{ideal} are the Gibbs free energies for surfaces with and without defects, respectively. They are calculated here including vibrational and electronic entropy [16] as well as zero-point corrections in harmonic approximation. The last term in Eq. 2 accounts for the stoichiometry changes, i.e., Δn_j is the difference in the number of atoms of species j, and μ_j the respective chemical potential. In case of hydrogen desorption, the H chemical potential change $\Delta\mu_{\mathrm{H}}$ with respect to an isolated molecule has been calculated in the approximation of a two-atomic ideal gas in dependence on partial pressure p and temperature T following

$$\Delta\mu_{\mathrm{H}}(p,T) = -k_B T \left[\ln\left(\frac{p\lambda^3}{k_B T}\right) - \ln\left(Z_{\mathrm{rot}}\right) - \ln\left(Z_{\mathrm{vib}}\right) \right], \tag{3}$$

where Z_{rot} and Z_{vib} are the rotational and vibrational partition functions, respectively; and λ the de Broglie thermal wavelength of the H_2 molecule,

$$\lambda = \sqrt{\frac{2\pi\hbar^2}{m k_B T}}. \tag{4}$$

IV. SURFACE CHARACTERIZATION AND FERMI LEVEL PINNING

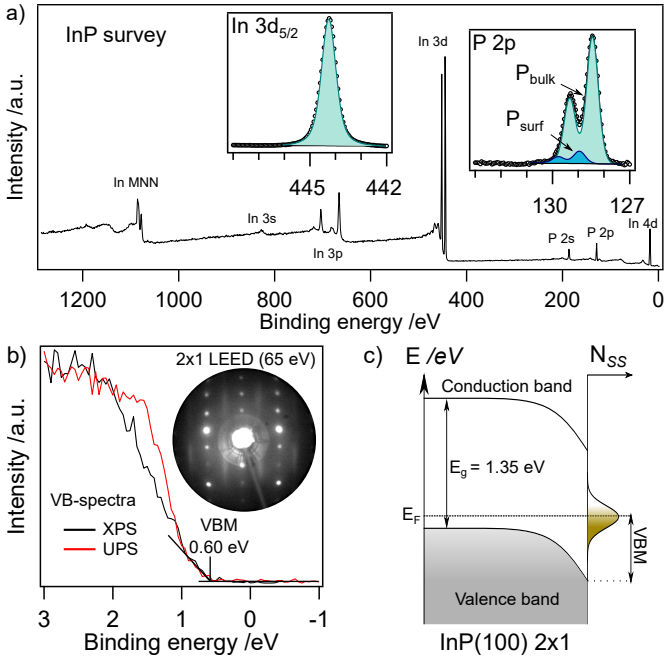

FIG. 1. XP survey spectra of the prepared InP(001) surface with detail scans of In $3d_{5/2}$ and P 2p, including a surface component fit (a). XPS and UPS valence band cut-offs with surface LEED pattern at 65 eV (b). Scheme of surface band bending due to surface states distribution N_{SS} according to experimentally evaluated Fermi level E_F to valence band distances VBM depicted in (c).

The XP survey scan of the as-grown P-rich InP(001) surface reveals a very clean surface only showing emissions from In and P (Fig. 1a). Especially, no traces of oxygen nor carbon can be found at binding energy BE(O 1s) ≈ 530 eV and BE(C 1s) ≈ 285 eV. The In $3d_{5/2}$ emission is located at 444.25 eV and can be fitted with a single Voigt line, indicating a homogeneous compound surface with no oxidized or segregated subspecies. The associated P 2p emission clearly contains a surface component which appears about 0.51 eV towards higher binding energies than the bulk-related emission at 128.45 eV with a relative intensity of ≈ 9%. We attribute this surface component to P dimers at the reconstructed surface [17]. Surface core level shifts as measured in high resolution synchrotron induced photoelectron spectroscopy are not resolved due to their low binding energy shifts ≤ 0.3 eV [18]. Furthermore, the low energy electron diffraction (LEED) patterns clearly reveal a 2×1 surface reconstruction, where the first order spots are separated by diffuse streaks along the [110] direction (Fig. 1b). The stabilization of buckled P dimers with atomic hydrogen can be arranged in-phase, resulting in a p(2×2) unit cell or out-of-phase corresponding to a c(4×2) unit cell [19, 20]. The superposition of both unit cells leads to the 2×1-like LEED pattern with the characteristic streaks in the ×2 half-order indicating a 2×2-2D-2H (2 buckled P dimers with 2 atomic hydrogen) surface reconstruction at the present surface as predicted from *ab initio* calculations [21]. For this very clean and homogeneous surface, the valence band maximum (VBM) is found to be at 0.60 eV, leading to a Fermi level position at the surface located slightly below mid-gap. However, according to the doping concentration of the grown InP with Zinc as shallow acceptor of about $N_A = 2 \cdot 10^{-18}$ cm^{-3}, the Fermi level in the bulk is expected to be around 40 meV above the VBM. The discrepancy between measured and calculated Fermi level position relative to the valence band indicates a strong surface band bending of $V_{BB} = 0.56$ eV due to apparent surface states inducing electrons into the surface which pin the Fermi level as depicted in Figure 1c. Considering a parabolic potential drop inside the InP space charge region (SCR), the amount of total surface charges Q_{SS} can be calculated with Eq. 5, meaning that < 1 % of the surface atoms contribute to a charged defect.

$$-Q_{SS} = \sqrt{2\varepsilon\varepsilon_0 q V_{BB} N_A} = 3.9 \cdot 10^{12}/cm \qquad (5)$$

This raises the question, what surface defect originates the initial surface band bending.

V. HYDROGEN RELATED SURFACE DEFECTS

Atomic hydrogen is known to stabilize the InP(001) 2×2-2D-2H (Fig. 6 left) surface, leading to completely filled and empty surface states close to the InP valence and conduction band egdes, respectively, even though an

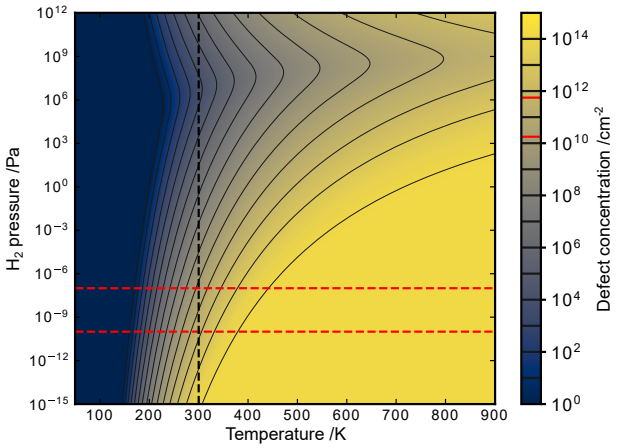

FIG. 2. Hydrogen vacancy concentration on a InP (2×2)-2D-2H surface as a function of pressure and temperature. The black and red dashed lines depict room temperature and the ultra-high vacuum range, respectively. The intersects of the dashed lines are depicted in the color bar by the red marks.

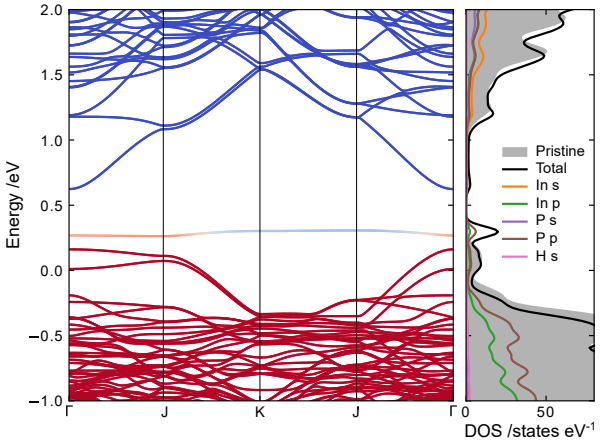

FIG. 3. Band structure and atomic as well as orbital resolved electronic density of states of the InP (2×2)-2D-1H surface. The red/blue lines correspond to occupied/unoccupied bands. The energy of zero corresponds to the InP bulk valence band maximum.

occupied surface band is located slightly above the valence band [22]. For that reason, the observed Fermi level pinning at mid-gap has to result from surface defects inducing electronic states within the bandgap of InP. Starting from the 2×2-2D-2H surface, we consider four types of hydrogen related defects, namely desorption and adsorption of one or two H atoms, respectively. The total probability of any of these defects can be calculated from Eq. 1, which is shown in dependence on temperature and partial H_2 pressure in Fig. 2. At room temperature and for a hydrogen partial pressure in the range of 10^{-10} to 10^{-7} Pa, a surface defect density in the order of 10^{10}

to 10^{12} cm^{-2} can be expected. This is sufficient to lead to surface band bending and is in good agreement with the calculated surface charges experimentally evaluated from Eq. 5. The desorption of one hydrogen atom from the 2D-2H surface is the by far predominant defect type under these conditions, leaving one phosphorous dangling bond at the surface. It corresponds to the formation of the InP(001) 2×2-2D-1H surface shown in Fig. 6 (right).

How do the surface electronic properties change upon H desorption? The band structure and the electron density of states (DOS) for the 2D-1H surface is shown in Fig. 4. It reveals that the H vacancy gives rise to an in-gap surface state feature. The atom-resolved DOS demonstrates that this state is of p character and is primarily due the partially filled P dangling bonds. In comparison to the valence band spectra, the dangling bond feature is located slightly below the calculated mid-gap position, which is in good agreement to our photoemission spectra, indicating that the surface P dangling bond is the dominating defect causing the Fermi level pinning at the present P-rich InP(001) surface.

VI. WATER ADSORPTION

In a next step, the surface reactivity of the observed surface states upon water adsorption has been investigated experimentally. For that purpose, the sample substrate was cooled with liquid nitrogen, and water from the gas phase was stepwise adsorbed by controlling water partial pressure and exposure time. As a final step, the cooling was stopped and the sample was measured at room temperature again.

After each step of exposure, XPS and UPS ($h\nu$(HeII) = 40.81 eV) measurements were conducted subsequently (Fig. 5). The XP spectra clearly show a core level shift of In $3d_{5/2}$ and P 2p towards lower binding energies of about 0.27 eV after cooling the surface. This shift cannot be only explained by a freeze-out of acceptor states, shifting the Fermi level into the VBM at this temperature. Moreover, the cryogenic temperature pronounces source-induced surface photovoltages because Shockley-Read-Hall recombination over surface states is reduced as described elsewhere [23–26]. After the step-wise adsorption of water, both core levels reveal a shift toward higher binding energies and get damped by the growing water layer, rising the O 1s signal at ≈ 533 eV. As the shift shows a linear dependence on the water coverage even in the multi-layer regime (> 1 L), we attribute it to a charging effect of the surface when the insulating ice-layer charges due to the emission of photoelectrons. However, the water adsorption itself does not lead to any spectral changes in the core level lines, indicating a chemically immune surface upon water adsorption. After warming up the surface back to room temperature, the water fully desorbs from the surface and no O 1s emission remains to be observed. At the same time, the In and P core

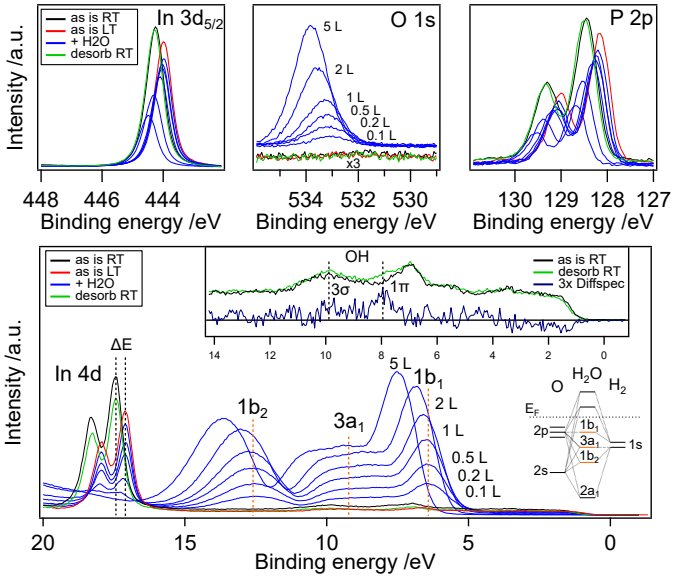

FIG. 4. XP core level ($h\nu$ = 1486.74 eV, top) and monochromatic HeII-spectra ($h\nu$ = 40.81 eV, bottom) of low temperature water adsorption on InP(001). Difference spectrum of valence band before and after water adsorption as well as LCAO-approach of molecular water have been inset in UP spectra.

levels shift back to their initial energy positions and no spectral changes are visible. With the HeII UP spectra, a very surface sensitive In 4d emission spectrum can be measured (Fig. 5 bottom). After cooling, the 4d core level shifts about ΔE = 0.33 eV towards the Fermi level, similar as observed from the XP core levels. With higher water coverage, a characteristic water feature arises in the valence band with 3 features which can be attributed to the $1b_1$ (6.5 eV), $3a_1$ (8.5 eV) and $1b_2$ (12.5 eV) highest occupied molecular orbitals of molecular water [27]. The water features shift to higher binding energies with increasing coverage, indicating charging of the water layer similar as also observed by XPS. In contrast to the XP spectra, the In 4d line seems to be unaffected by the water layer. Only for coverages > 1 L, the In 4d line slightly shifts to higher binding energies, confirming that all core level shifts are source dependent and can be related to the charging of the topmost ice layer. Even though the photon flux of the monochromatized HeII-source (≈ 10^{11} Photons/s/mm^2) is in the range of the XPS-source, the HeII measurement is less susceptible to charging as the lower photon energy leads to less photoionization. After the desorption of the ice layers, the UP spectra reveal only slight spectral changes. However, at 8.0 eV and 9.9 eV, two features appear in the difference spectra, which might be assigned to 1π and 3σ bonds of adsorbed OH groups [27, 28], indicating a dissociation of adsorbed H_2O. Dissociative water adsorption has been reported for the InP(110) [29] as well as for the In-rich InP(001) surface [3, 30]. However, the weak signal in UPS and no

signal in the XPS O 1s line indicates that OH is only present at a few surface sites far below a monolayer coverage. Furthermore, the LEED pattern still exhibits the 2×1 surface reconstruction, indicating that there are no structural changes after the desorption of water. As a conclusion from our experimental data, we state that starting from a defective P-rich InP(001) surface, almost no electronic interaction with chemical bond formation to water is observed.

In order to verify our experimental findings, we determined the water adsorption configuration for the ideal 2×2-2D-2H and the hydrogen deficient surfaces computationally. The potential energy surface (PES) for single H_2O molecules adsorbed on the InP(001) 2×2-2D-2H surface is shown in Fig. 6 (left). Interestingly, the P dimer is not a favorable bonding site for water. This agrees with earlier findings for In-rich InP surfaces [30, 31], where water adsorbs at In rather than on P sites. Here, the molecule preferably sits in the trench between the P dimer rows. In Figure 7, the equilibrium bonding geometry of a surface adsorbed water molecule is shown together with the calculated charge redistribution upon adsorption. There is a slight charge accumulation between the water proton and the P dimer up-atom, and a somewhat weaker charge accumulation between water oxygen and second-layer In atom, leading to a weak physisorption. However, neither the atomic structure nor the electronic properties of the InP(001) 2×2-2D-2H surface are strongly affected by the water adsorption. In particular, water adsorption does not give rise to additional gap states.

Interestingly, the computational findings are very similar for the hydrogen deficient, i.e. the InP(001) 2×2-2D-1H surface. However, compared to water adsorption on the 2×2-2D-2H surface, a slightly larger (by about 0.03 eV) adsorption energy is calculated. The calculated PES indicates again adsorption preferentially in the trench between the P dimer rows (Fig. 6 (right)). Here, the H_2O molecule bonds weakly to the P dimer, which is partially H saturated. For that reason, the electronic mid-gap state resulting from H desorption is not affected by water adsorption, confirming our experimental results, according to which no electronic nor chemical reactions could be identified upon the adsorption of molecular water.

The situation changes, however, as soon as water dissociation is considered. According to our experimental results, we could confirm slight traces of OH remaining after the desorption of molecular water. In Figure 8, the PES calculated for OH adsorbed on InP(001) 2×2-2D-2H (left) and 2×2-2D-1H (right) is shown. Here the adsorption energy is calculated with respect to molecular water, and is obtained as

$$E_{\mathrm{ads}}(\mathrm{OH}) = E_{\mathrm{total}} - E_{\mathrm{clean}} - E_{\mathrm{OH}} \qquad (6)$$

with

$$E_{\mathrm{OH}} = E_{\mathrm{H_2O}} - \frac{1}{2}E_{\mathrm{H_2}}. \qquad (7)$$

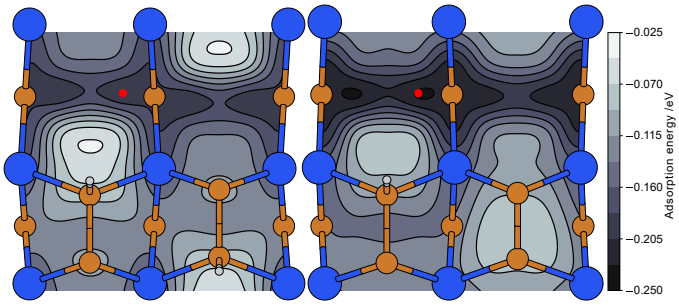

FIG. 5. Calculated potential energy surfaces for single water molecules on InP(001)(2×2) 2D-2H (left) and 2D-1H (right) surfaces. The red marks correspond to the most favorable adsorption sites. Blue and orange spheres indicate In and P, respectively.

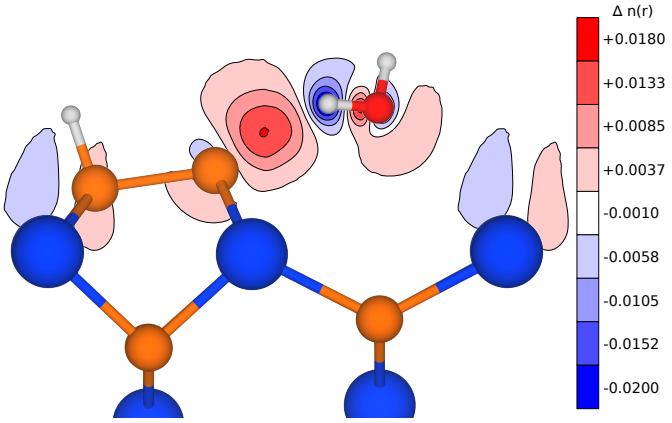

FIG. 6. Structural configuration and water-induced charge redistribution for water adsorbed on 2D-2H. Red and blue isosurfaces indicate regions of charge accumulation and depletion, respectively.

The calculations shown in Fig. 8 indicate that OH adsorption is favorable on the defective 2×2-2D-1H surface, but not at all on 2×2-2D-2H. With that, the observed OH groups in the UP spectra could further indicate apparent P dangling bonds at the prepared InP(001) surface. In case of the 2D-1H surface, the hydroxyl group adsorbs on the P dimer dangling bond, saturating the half-filled dangling P orbital resulting from H desorption. Accordingly, the mid-gap surface state is removed and the band structure resembles that of the surface without defects. It should be noted that the P dangling bond does not only change the adsorption energy at the dangling bond site itself, but on all P atoms of the 2×2-2D-1H surface lattice.

Even though the UP spectra reveal adsorbed OH groups at the surface, the Fermi level position within the bandgap, and with that the surface band bending, remain unaffected after the adsorption of water, indicating that not all dangling bond defects could be passivated by the OH groups. This also confirms that the P dangling bond center itself is not the active site for water

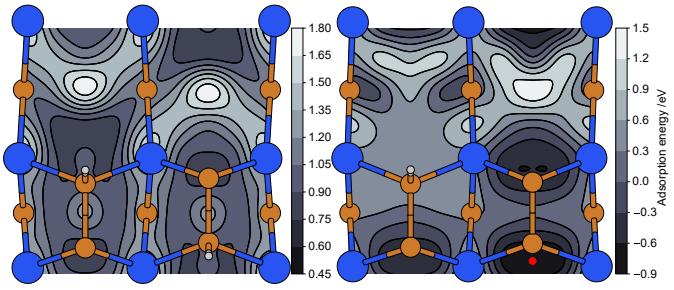

FIG. 7. Calculated potential energy surfaces for hydoxyl group adsorption on InP(001)(2×2) 2D-2H (left) and 2D-1H (right) surfaces. The red mark correspond to the most favorable adsorption site.

dissociation. The dissociation of molecular water on InP surfaces requires free In sites as recently shown for In-rich InP(001) surface [30]. For that reason, we suggest that water dissociation only occurs at step edges rather than on terraces of the P-rich InP(001) surface.

As a future perspective, additional experiments are planned exposing the P-rich InP(001) surface to acidic and basic aqueous solutions offering solvated H^+ or OH^- ions, which may strongly interact chemically to separated defect sites and may lead to a complete electronic surface passivation.

VII. CONCLUSION

P-rich InP(001) was investigated by photoemission spectroscopy as well as DFT calculations. We found a strong surface band bending, which we attributed to hydrogen vacancies, leading to P dangling bonds and induce half filled mid-gap surface states. Low temperature water adsorption could not reveal a strong interaction of the molecular water with the present InP(001) surface. Our computational results could confirm that the considered dangling bond defect does not significantly change the adsorption behavior of the InP(001) surface compared to the hydrogen saturated surface. After the desorption of molecular water, we could only find traces of remaining OH groups at the InP(001) surface, indicating a partial dissociation of the water molecule. Potential-energy surface calculation reveal that in contrast to H_2O, P dangling bonds strongly change the adsorption behavior of OH, which is able to passivate the mid-gap state after bonding to the dangling bond site. However, the remaining Fermi level pinning after water adsorption indicate that P dangling bonds are not the active sites for water dissociation on P-rich InP(001) surfaces as neighboring active sites for H_2O cleavage are missing.

VIII. ACKNOWLEDGMENTS

Financial support by DFG (PAK981: Project No. JA859/35-1, SCHM1361/26, and HA3096/14-1) is gratefully acknowledged. The authors thank the Paderborn Center for Parallel Computing (PC^2) and the Höchstleistungs-Rechenzentrum Stuttgart (HLRS) for grants of high-performance computing time.

[1] W.-H. Cheng, M. H. Richter, M. M. May, J. Ohlmann, D. Lackner, F. Dimroth, T. Hannappel, H. A. Atwater, and H.-J. Lewerenz, Monolithic Photoelectrochemical Device for Direct Water Splitting with 19% Efficiency, ACS Energy Letters **3**, 1795 (2018).

[2] L. Gao, Y. Cui, R. H. Vervuurt, D. Van Dam, R. P. Van Veldhoven, J. P. Hofmann, A. A. Bol, J. E. Haverkort, P. H. Notten, E. P. Bakkers, and E. J. Hensen, High-efficiency InP-based photocathode for hydrogen production by interface energetics design and photon management, Advanced Functional Materials **26**, 679 (2016).

[3] M. M. May, H.-J. Lewerenz, and T. Hannappel, Optical in Situ Study of InP(100) Surface Chemistry: Dissociative Adsorption of Water and Oxygen, The Journal of Physical Chemistry C **118**, 19032 (2014).

[4] A. Hajduk, M. V. Lebedev, B. Kaiser, and W. Jaegermann, Interaction of liquid water with the p-$GaInP_2$(100) surface covered with submonolayer oxide, Physical Chemistry Chemical Physics **20**, 21144 (2018).

[5] J. Klett, B. Elger, S. Krähling, B. Kaiser, W. Jaegermann, and R. Schäfer, Water dissociation on silica in the presence of atomic platinum, Applied Surface Science **375**, 85 (2016).

[6] A. C. Bronneberg, C. Höhn, and R. Van De Krol, Probing the Interfacial Chemistry of Ultrathin ALD-Grown TiO_2 Films: An In-Line XPS Study, Journal of Physical Chemistry C **121**, 5531 (2017).

[7] T. Cottre, M. Fingerle, M. Kranz, T. Mayer, B. Kaiser, and W. Jaegermann, Interaction of Water with Atomic Layer Deposited Titanium Dioxide on p-Si Photocathode: Modeling of Photoelectrochemical Interfaces in Ultrahigh Vacuum with Cryo-Photoelectron Spectroscopy, Advanced Materials Interfaces **8**, 2002257 (2021).

[8] M. Fingerle, S. Tengeler, W. Calvet, T. Mayer, and W. Jaegermann, Water Interaction with Sputter-Deposited Nickel Oxide on n-Si Photoanode: Cryo Photoelectron Spectroscopy on Adsorbed Water in the Frozen Electrolyte Approach, Journal of The Electrochemical Society **165**, H3148 (2018).

[9] T. Hannappel, L. Töben, K. Möller, and F. Willig, In-situ monitoring of InP(100) and GaP(100) interfaces and characterization with RDS at 20 K, Journal of Electronic Materials 2001 30:11 **30**, 1425 (2001).

[10] T. Letzig, H. J. Schimper, T. Hannappel, and F. Willig, P-H bonds in the surface unit cell of P-rich ordered InP(001) grown by metalorganic chemical vapor deposition, Physical Review B - Condensed Matter and Ma-

terials Physics **71**, 033308 (2005).
[11] T. Hannappel, S. Visbeck, L. Töben, and F. Willig, Apparatus for investigating metalorganic chemical vapor deposition-grown semiconductors with ultrahigh-vacuum based techniques, Review of Scientific Instruments **75**, 1297 (2004).
[12] G. Kresse and J. Furthmüller, Efficiency of ab-initio total energy calculations for metals and semiconductors using a plane-wave basis set, Computational Materials Science **6**, 15 (1996).
[13] J. P. Perdew, K. Burke, and M. Ernzerhof, Generalized Gradient Approximation Made Simple, Physical Review Letters **77** (1996).
[14] P. E. Blöchl, Projector augmented-wave method, Phys. Rev. B **50**, 17953 (1994).
[15] G. Kresse and D. Joubert, From ultrasoft pseudopotentials to the projector augmented-wave method, Physical Review B **59**, 1758 (1999).
[16] S. Wippermann and W. G. Schmidt, Entropy explains metal-insulator transition of the Si(111)-in nanowire array, Physical Review Letters **105**, 126102 (2010).
[17] P. Vogt, A. M. Frisch, T. Hannappel, S. Visbeck, F. Willig, C. Jung, R. Follath, W. Braun, W. Richter, and N. Esser, Atomic structure and composition of the P-rich InP(001) surfaces, Applied Surface Science **166**, 190 (2000).
[18] W. G. Wilke, V. Hinkel, W. Theis, and K. Horn, Surface core-level shifts on InP(110): Experiments and Madelung energy calculations, Physical Review B **40**, 15.
[19] L. Li, B.-K. Han, Q. Fu, and R. F. Hicks, Example of a Compound Semiconductor Surface that Mimics Silicon: The InP(001)-(2 x 1) Reconstruction, Physical Review Letters **82**, 1879 (1999).
[20] P. Kleinschmidt, H. Döscher, P. Vogt, and T. Hannappel, Direct observation of dimer flipping at the hydrogen-stabilized GaP(100) and InP(100) surfaces, Physical Review B **83**, 155316 (2011).
[21] W. G. Schmidt, P. H. Hahn, F. Bechstedt, N. Esser, P. Vogt, A. Wange, and W. Richter, InP(001)-(2 x 1) Surface: A Hydrogen Stabilized Structure, Physical Review Letters **90**, 4 (2003).
[22] P. H. Hahn and W. G. Schmidt, Surface Ordering of P-rich InP(001): Hydrogen Stabilization vs Electron Correlation, Surface Review and Letters **10**, 163 (2003).
[23] M. Alonso, R. Cimino, and K. Horn, Surface photovoltage effects in photoemission from metal-GaP(110) interfaces: Importance for band bending evaluation, Physical Review Letters **64**, 1947 (1990).
[24] A. Schellenberger, R. Schlaf, C. Pettenkofer, and W. Jaegermann, Synchrotron-induced surface-photovoltage saturation at intercalated Na/WSe_2, Physical Review B **45**, 3538 (1992).
[25] L. Kronik and Y. Shapira, Surface photovoltage phenomena: Theory, experiment, and applications, Surface Science Reports **37**, 1 (1999).
[26] M. V. Lebedev, G. M. Savchenko, N. S. Averkiev, A. Hajduk, B. Kaiser, and W. Jaegermann, Surface potential in n- and p-$GaInP_2$(100): temperature effect, Journal of Physics D: Applied Physics **54**, 185104 (2021).
[27] W. Jaegermann and T. Mayer, *Landolt-Börnstein*, edited by H. Bonzel, Landolt-Börnstein - Group III Condensed Matter, Vol. 42A4 (Springer-Verlag, Berlin/Heidelberg, 2005) pp. 226–298.
[28] C. Larsson and A. Flodström, Dissociative H2O adsorption on the Si (100) 2×1 and Ge (100) 2×1 surfaces, Vacuum **42**, 297 (1991).
[29] O. Henrion, A. Klein, and W. Jaegermann, Water adsorption on UHV cleaved InP(110) surfaces, Surface Science **457**, 337 (2000).
[30] I. A. Alvarado Ruiz and W. G. Schmidt, Water/InP(001) from Density Functional Theory, ACS Omega **7**, 19355 (2022).
[31] B. C. Wood, E. Schwegler, W. I. Choi, and T. Ogitsu, Surface chemistry of GaP(001) and InP(001) in contact with water, Journal of Physical Chemistry C **118**, 1062 (2014).